A Fast Scheme to Calculate Electronic Couplings between P3HT Polymer Units Using Diabatic Orbitals for Charge Transfer Dynamics Simulations

Tao Yu, *[a] Florence Fabunmi,[a] Jingsong Huang, [b] Bobby G. Sumpter, [b] and Jacek Jakowski *[b]

We propose a fast and accurate calculation method to compute the electronic couplings between molecular units in a thiophene-ring-based polymer chain mimicking a real organic semiconducting polymer, poly(3-hexylthiophene). Through a unit block diabatization scheme, the method employed minimal number of diabatic orbitals to compute the site energies and electronic couplings, which were validated by comparing with benchmark density functional theory calculations. In addition, by using the obtained electronic couplings, a quantum dynamics simulation was carried out to propagate a hole initially localized in a thiophene-ring unit of the polymer chain. This work establishes a simple, efficient, and robust means for the simulation of electron or hole transfer processes in organic semiconducting materials, an important capability for study and understanding of the class of organic optoelectronic and photovoltaic materials. © 2018 Wiley Periodicals, Inc.

DOI:10.1002/jcc.25749

Introduction

For many years, organic solar cells (OSCs) constructed by organic semiconductors have been demonstrated to show encouraging light-to-electricity conversion efficiency and can be considered as a promising potential source of renewable electrical energy.[1–4] Compared with solar cells based on inorganic materials, OSCs display a number of advantages, such as lower cost, flexibility for easy processing and fabrication, as well as easily tunable properties through synthetic modification. One of the key profiles of organic semiconductors is that the building-block molecule contains conjugated π orbitals, which are electronically coupled with each other. In particular, P3HT[4–6] is one of the prototypical materials in the organic semiconductor family.[7] The conductivity of P3HT lies on its conjugated thiophene-ring segments. The π-conjugated orbitals of the neighboring thiophenes in the P3HT chain couple together into delocalized orbitals, which extend along the P3HT chain and, for infinitely long chains, form electronic bands. Contrary to this, the coupling between thiophene units that belong to different chains in crystalline P3HT is weak, which prevents formation of extended orbitals delocalized across multiple different chains.

Many experimental and theoretical studies have investigated the mechanism and physical driving forces for charge transfer (CT) in organic crystals of semiconducting polymers.[8–12] In general, two mechanisms are considered for CT in organic materials: (1) band transport mechanism, and (2) charge hopping mechanism. One of the most important physical characteristics that determine the nature of charge carrier transport *within* or *between* P3HT polymer chains comes from electronic couplings (ECs) between the nearby thiophene rings. Strong coupling, such as between neighboring thiophene units *within* a P3HT chain, leads to fast band transport. Weak coupling, such as between thiophene units that belong to *different* P3HT chains, leads to a charge hopping mechanism. While it is tempting to use solid-state density functional theory (DFT) approaches designed to model electronic structure in crystals and exploit its periodicity, crystalline P3HT is far from an ideal crystal. Rather, its shows a high level of polycrystallinity with a large number of very small, nanometer sized crystal grains. It has been observed that the maximum crystallinity of P3HT is achieved when the molecular mass of individual P3HT chains is about 10,000 mass units, which correspond to about ~60 thiophene units.[13] Polycrystallinity and grain boundaries greatly affect the charge transport properties of bulk P3HT.[12,14] The same is true for other organic materials.

[a] *T. Yu, F. Fabunmi*
Department of Chemistry, Tennessee Technological University, Cookeville, Tennessee, 38501
E-mail: tyu@tntech.edu
[b] *J. Huang, B. G. Sumpter, J. Jakowski*
Center of Nanophase Materials Sciences & Computational Sciences and Engineering Division, Oak Ridge National Laboratory, Oak Ridge, Tennessee, 37831
E-mail: jakowskij@ornl.gov

Contract Grant sponsor: Oak Ridge National Laboratory; Contract Grant number: ERKCZ01

It is challenging to compute the EC and CT dynamics for the entire polymer system. Quantum chemical studies are typically limited, within a static picture, to a few units of a given polymer and to the analysis of the highest occupied molecular orbitals (HOMOs) and lowest unoccupied molecular orbitals (LUMOs). A commonly used method to approximately obtain the EC in organic crystals is to calculate the HOMO and LUMO associated energy gaps using a single unit molecule or segment.[8–10,15] However, a-few-units approximation does not describe adequately the formation of electronic bands which in consequence leads to overestimated band gaps. A cure for that would be to extend the length of polymer and increase the number of constituent segments. But the number of basis functions quickly increases and becomes too large for routine treatment with electronic structure DFT codes due to its cubic scaling with the number of basis functions. For example, the modest 6-31G(d) basis set[16–19] requires nearly 200 basis functions for a single hexyl-thiophene unit, a building block of P3HT. In a typical P3HT crystal a single polymer chain consists of ~60 hexyl-thiophene units and thus would require 12,000 basis functions for a *single* chain, let alone a crystal grain that contains many chains.

Here, we present and benchmark a simplified DFT approach in which the orbitals of the valence and conduction bands in full DFT calculations based on STO-3G and 6-31G(d) basis sets, are re-constructed from a small number of molecular orbitals calculated for independent units. We revisit the EC calculations by directly working on a model P3HT polymer chain with 64 thiophene units using "relevant" localized diabatic orbitals obtained by a unit block diagonalization scheme.[20–22] By this scheme, both the EC between thiophene and site energy (SE) of each thiophene in the molecule chain were obtained simultaneously in an efficient way. These quantities can also be used to carry out CT kinetics and dynamics simulations. Note that the proposed method is a generic one that can be used to study any organic semiconductor or organic crystal system with even a very large number of molecules and obtain the EC values on-the-fly with a reasonable inexpensive cost. Furthermore, we employ the obtained site energies and couplings to carry out a quantum dynamics simulation of propagating a hole initially localized in one unit along the chain.

Methodology for Construction of Diabatic Orbitals for Charge Transport Modeling

Here we discuss the systematic procedure for decomposing a set of delocalized valence and conduction band orbitals onto a small subset of localized diabatic orbitals.

We pose the following questions: Can the small number of frontier orbitals that represent localized diabatic states of individual thiophenes be used to reproduce adequately and in a numerically robust way the delocalized π-conjugated molecular orbitals of valence and conduction bands in polythiophene? What is the systematic and optimal procedure in terms of accuracy versus computational cost? The positive answers to these questions can allow large scale quantum dynamical simulations at a minimal computational cost. We postulate that one can use a small number of the diabatic localized states to generate a good quality delocalized state with arbitrary accuracy. Our approach draws from Wannier's procedure[23–25] to construct maximally localized orbitals and from the density functional tight-binding approach to generate tight binding parameters.[26–29] We also note that this procedure is similar to calculating CT integrals in photovoltaic devices.[11,30]

We use the top-down approach. That is, we start from the converged full DFT calculations with the localized atomic orbitals basis set for the long polythiophene chain. We then systematically remove blocks in the Hamiltonian and overlap matrices that correspond to coupling between the most remote thiophenes while monitoring the effect of truncation on the accuracy for description of valence and conduction orbitals. Regardless of the specific DFT functional and basis set used, the DFT Kohn–Sham equation in atomic orbitals

$$HC = SCE \tag{1}$$

can always be written in the block-matrix-decomposed form as:

$$\begin{pmatrix} H_{A_1} & V_{1,2} & V_{1,3} & \cdots & \cdots & V_{1,N} \\ V_{2,1} & H_{A_2} & V_{2,3} & \ddots & & \vdots \\ V_{3,1} & V_{3,2} & H_{A_3} & \ddots & \ddots & \vdots \\ \vdots & & \ddots & \ddots & V_{N-2,N-1} & V_{N-2,N} \\ \vdots & & & & H_{A_{N-1}} & V_{N-1,N} \\ V_{N,1} & \cdots & \cdots & \cdots & V_{N,N-1} & H_{A_N} \end{pmatrix} \begin{pmatrix} C_1 \\ C_2 \\ \cdot \\ \cdot \\ C_N \end{pmatrix} = E \begin{pmatrix} S_{A_1} & S_{1,2} & S_{1,3} & \cdots & \cdots & S_{1,N} \\ S_{2,1} & S_{A_2} & S_{2,3} & \ddots & & \vdots \\ S_{3,1} & S_{3,2} & S_{A_3} & \ddots & \ddots & \vdots \\ \vdots & & \ddots & \ddots & S_{N-2,N-1} & S_{N-2,N} \\ \vdots & & & & S_{A_{N-1}} & S_{N-1,N} \\ S_{N,1} & \cdots & \cdots & \cdots & S_{N,N-1} & S_{A_N} \end{pmatrix} \begin{pmatrix} C_1 \\ C_2 \\ \cdot \\ \cdot \\ C_N \end{pmatrix} \tag{2}$$

where the diagonal terms H_{A_k} and S_{A_k} correspond to Hamiltonian and overlap matrix blocks unit out of all N thiophene units. The diagonal blocks H_{A_k} and S_{A_k} are square and of the size $N^k_{\text{basis}} \times N^k_{\text{basis}}$ where N^k_{basis} is the number of localized atomic orbitals basis functions for the k-th fragment and can vary from fragment to fragment for copolymers. The non-diagonal terms $V_{k,l}$ and $S_{k,l}$ describe Hamiltonian coupling and overlap between k-th and l-th fragments and are rectangular blocks of the size $N^k_{\text{basis}} \times N^l_{\text{basis}}$. For the polythiophene case, all fragments have the same size, and the corresponding overlap and coupling matrices are square.

The H and S matrices contain information about all orbitals including core, valence, and virtual orbitals and are in principle large matrices. The diagonal blocks H_{A_k} for the k-th fragment also contain a mean-field information about the remaining part of the system. That is, the one-electron Hamiltonian for k-th

unit includes integrals between atomic orbitals (A.O.) localized on the k-th unit with all other nuclei. Similarly, the two-electron Hamiltonian is built from the total density matrix and includes interaction between electrons localized in the k-th unit and those in other units. The column vector C is an eigenvector (molecular orbital) of H with corresponding eigenvalue E (orbital energy). The size of the matrix H and S is equal to the sum of basis functions of each constituent fragments:

$$\dim(H) = \dim(S) = \sum_{k=1}^{N} N_{\text{basis}}^{k} \tag{3}$$

where k enumerates fragments and N_{basis}^{k} is the number of its basis functions. In principle, dim(H) depends on the specific basis set used and can be very large for multiple-zeta basis sets with polarization and diffuse components included.

We note that the eigenstates of H_{A_k} blocks form a new basis set of orbitals localized within a k-th unit

$$H_{A_k} B_k = \varepsilon_{Ak} S_{A_k} B_k \tag{4}$$

with B_k representing a set N_{basis}^{k} eigenvectors for k-th block, and ε_{Ak} being a diagonal matrix of the corresponding eigenvalues. A superposition of B_k for all k forms a diabatic basis set, $B = \{B_1, B_2, \ldots B_N\}$, that formally spawns the same vector space as the original A.O. basis set and is equivalent to it. In the matrix form the diabatic basis set, B, is block diagonal and given by:

$$B = \begin{bmatrix} B_1 & 0 & 0 \\ 0 & \ddots B_k \ddots & 0 \\ 0 & 0 & B_N \end{bmatrix} \tag{5}$$

Our Kohn–Sham equations transformed from the localized A.O. basis set to the diabatic basis set becomes:

$$\overline{H}\overline{C} = \overline{S}\overline{C}E \tag{6}$$

or in an expanded form:

$$\begin{pmatrix} \varepsilon_{A_1} & \overline{V}_{1,2} & \overline{V}_{1,3} & \cdots & \cdots & \overline{V}_{1,N} \\ \overline{V}_{2,1} & \varepsilon_{A_2} & \overline{V}_{2,3} & & & \vdots \\ \overline{V}_{3,1} & \overline{V}_{3,2} & \ddots & \ddots & & \vdots \\ \vdots & & \ddots & \varepsilon_{A_{N-2}} & \overline{V}_{N-2,N-1} & \overline{V}_{N-2,N} \\ \vdots & & & \overline{V}_{N-1,N-2} & \varepsilon_{A_{N-1}} & \overline{V}_{N-1,N} \\ \overline{V}_{N,1} & \cdots & \cdots & \overline{V}_{N,N-2} & \overline{V}_{N,N-1} & \varepsilon_{A_N} \end{pmatrix} \begin{pmatrix} \overline{C}_1 \\ \overline{C}_2 \\ \vdots \\ \overline{C}_N \end{pmatrix}$$

$$= E \begin{pmatrix} I_1 & \overline{S}_{1,2} & \overline{S}_{1,3} & \cdots & \cdots & \overline{S}_{1,N} \\ \overline{S}_{2,1} & I_2 & \overline{S}_{2,3} & & & \vdots \\ \overline{S}_{3,1} & \overline{S}_{3,2} & \ddots & \ddots & & \vdots \\ \vdots & & \ddots & I_{N-2} & \overline{S}_{N-2,N-1} & \overline{S}_{N-2,N} \\ \vdots & & & \overline{S}_{N-1,N-2} & I_{N-1} & \overline{S}_{N-1,N} \\ \overline{S}_{N,1} & \cdots & \cdots & \overline{S}_{N,N-2} & \overline{S}_{N,N-1} & I_N \end{pmatrix} \begin{pmatrix} \overline{C}_1 \\ \overline{C}_2 \\ \vdots \\ \overline{C}_N \end{pmatrix} \tag{7}$$

The non-diagonal blocks in matrices $\overline{H}$ and $\overline{S}$ are calculated using B set of basis functions, $B = \{B_1, B_2, \ldots B_N\}$, as follows:

$$\overline{V}_{k,k'} = (0 \ldots B_k \ldots 0) \begin{pmatrix} H_{A_1} & V_{1,2} & V_{1,3} & \cdots & \cdots & V_{1,N} \\ V_{2,1} & H_{A_2} & V_{2,3} & \ddots & & \vdots \\ V_{3,1} & V_{3,2} & H_{A_3} & \ddots & \ddots & \vdots \\ \vdots & & \ddots & \ddots & V_{N-2,N-1} & V_{N-2,N} \\ \vdots & & & & H_{A_{N-1}} & V_{N-1,N} \\ V_{N,1} & \cdots & \cdots & \cdots & V_{N,N-1} & H_{A_N} \end{pmatrix} \begin{pmatrix} 0 \\ \vdots \\ B_{k'} \\ \vdots \\ 0 \end{pmatrix} \tag{8}$$

$$\overline{S}_{k,k'} = (0 \ldots B_k \ldots 0) \begin{pmatrix} S_{A_1} & S_{1,2} & S_{1,3} & \cdots & \cdots & S_{1,N} \\ S_{2,1} & S_{A_2} & S_{2,3} & \ddots & & \vdots \\ S_{3,1} & S_{3,2} & S_{A_3} & \ddots & \ddots & \vdots \\ \vdots & & \ddots & \ddots & S_{N-2,N-1} & S_{N-2,N} \\ \vdots & & & & S_{A_{N-1}} & S_{N-1,N} \\ S_{N,1} & \cdots & \cdots & \cdots & S_{N,N-1} & S_{A_N} \end{pmatrix} \begin{pmatrix} 0 \\ \vdots \\ B_{k'} \\ \vdots \\ 0 \end{pmatrix} \tag{9}$$

One can expect that the farther away two thiophene fragments k and k' are from each other, then the corresponding overlap matrix blocks $\overline{S}_{k,k'}$ and Hamiltonian blocks $\overline{H}_{k,k'}$ become smaller in magnitude hence less and less important. This allows reduction of the computational cost for evaluation of $\overline{S}$ and $\overline{H}$ matrices from quadratic scaling O(N^2) to linear scaling O(N) if the $\overline{S}_{k,k'}$ and $\overline{H}_{k,k'}$ blocks could be assumed to be zero and neglected for the separation between k and k' units larger than some threshold. In the process of "linearization" the $\overline{S}$ and $\overline{H}$ matrices become sparse and banded.

Equations (1,2) and (6,7) are equivalent, and the corresponding transformation is merely a basis set transformation from the localized A.O. basis set to the diabatic basis set. So far, no approximation has been made and therefore the diabatization scheme is exact. The advantage of the current diabatic basis set is twofold. First, it effectively decouples core electron orbitals and high energy virtual orbitals from the frontier orbitals. Second, the $\overline{S}_{k,k'}$ and $\overline{H}_{k,k'}$ blocks for units k and k' which are far apart are smaller and smaller and can likely be neglected. The resulting $\overline{S}$ and $\overline{H}$ matrices are sparse with the computational cost of their evaluation scaling linearly with the number N of units. The majority of chemically relevant processes such as bond breaking and formation or charge transport involve frontier orbitals only. The diabatic basis set provides a minimal basis set for description of frontier orbitals of the valence and conduction bands. The corresponding Hamiltonian, overlap, and density expressed in terms of the diabatic basis set are compact and much smaller than expressed in terms of the A.O. basis set. Such an optimized minimal basis set is suitable for a real-time modeling of electron dynamics in large molecular systems.

In the following section, we will discuss the computational model of valence and conduction bands of polythiophene in the diabatic representation for a realistic size of polymer chain and the effects of neglecting the non-diagonal $\overline{S}_{k,k'}$ and $\overline{H}_{k,k'}$ blocks on the accuracy. Finally, as an illustration, we will discuss

the hole transport dynamics in the valence band of polythiophene.

Computational Model for Valence and Conduction Bands of Polythiophene

The structure used in this work is based on the unit cell structure of the P3HT crystal.[31] Crystalline P3HT has a monoclinic crystal structure with the 87° tilt angle along stacking direction as shown in Figure 1a. Figure 1b shows a view of the thiophene chain backbone along the π-stacking direction (*x*-axis in Fig. 1b). In the current work we focus on electronic structure and dynamics within a single P3HT chain while completely neglecting inter-chain charge transport. Also, the hexyl arms of P3HT were removed for the purpose of the current studies, as they are not directly involved in charge transport and do not contribute to formation of valence and conduction bands. The main role of aliphatic hexyl arms of P3HT is to improve miscibility of the blends in the OSC devices.

Based on the crystallographic data for P3HT we constructed a realistic sized molecular structure of a single polythiophene chain with 64 thiophene units. This length of polythiophene corresponds to experimentally observed maximum crystallinity of P3HT at 10,000 mass units.[13] The two ends of the chain were capped with hydrogen atoms to passivate the dangling bonds, and the resulting structure is H-T_{64}-H, where T represents thiophene. By a little modification, removing the side-chain in each unit, making the thiophene ring coplanar (lies in *yz*-plane), and demanding the two neighboring rings preserve C_{2h} point group symmetry greatly simplify the analysis. The 64-unit chain was constructed by continuously translating the two neighboring units along the *z*-direction by 7.904 Å. Note that the artificially constructed chain was not meant to reproduce a P3HT single-chain. However, such a modification will not alter any physical analysis and conclusion presented below, but it provides a simple and clear picture for relevant π orbitals in the following discussion. The generated structure with 64 thiophene units is shown in Figure 1b.

We note that the valence and conduction band orbitals of polythiophene are all π-conjugated orbitals with planar symmetry. Each thiophene ring has five atoms (four carbons and one sulfur). Each atom contributes one valence p_x orbital to the

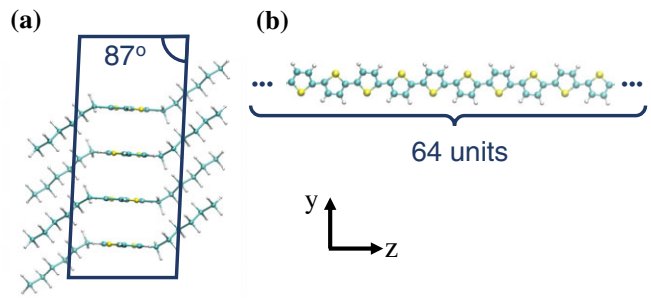

Figure 1. a) Along-chain view of the P3HT crystal (monoclinic). b) A snapshot of the thiophene-ring polymer chain with 64 units (only a segment is shown). The chain lies in the *yz*-plane with C_{2h} symmetry. Color scheme: yellow (sulfur atom); cyan (carbon atom); and white (hydrogen atom). [Color figure can be viewed at wileyonlinelibrary.com]

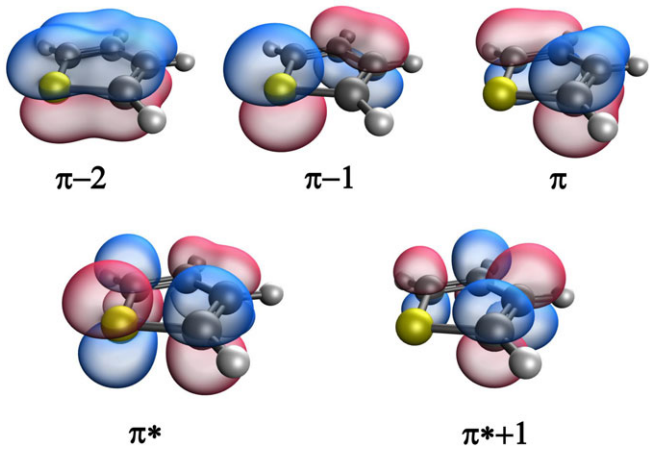

Figure 2. The five diabatic π orbitals of thiophene obtained from LRC-ωPBEh with the STO-3G basis set. Note the π-2 orbital corresponds to HOMO-5 in thiophene, whereas the orbitals from π-1 to π*+1 correspond to HOMO-1 to LUMO+1 in thiophene. [Color figure can be viewed at wileyonlinelibrary.com]

thiophene ring, which generates the basis for five diabatic π frontier orbitals per thiophene unit. Such π diabatic frontier orbitals obtained from the STO-3G basis set for a thiophene are shown in Figure 2. In the polythiophene chain consisting of *N* thiophene units, there are altogether $5 \times N$ orbitals in the valence and conduction bands, regardless of the type and size of the A.O. basis set used. Increasing the size of the A.O. basis set simply improves the description of the valence orbitals and of corresponding diabatic orbitals but does not change the number of valence and conduction band orbitals involved in chemical processes and charge transport. To put this into perspective, modeling valence and conduction band orbitals in a 64 unit long polythiophene requires only dealing with matrices of size 320×320 (five orbitals per thiophene times 64 thiophenes), whereas the full 6-31G(d) basis set for the same length P3HT requires dealing with ~$12{,}800 \times 12{,}800$ matrices (200 basis per unit).

We will now systematically analyze the effect of dropping the off-diagonal block elements $\overline{V}_{k,l}$ and $\overline{S}_{k,l}$ on the corresponding eigenvalues and eigenvectors in eq. (7). That is, we first solve the eigenproblem using the full Hamiltonian with all coupling blocks included. This solution serves as the frame of reference. We then remove the blocks $\overline{V}_{1,N}$, $\overline{V}_{N,1}$ and $\overline{S}_{1,N}$, $\overline{S}_{N,1}$ in the Hamiltonian and overlap matrices and calculate the eigenvalues and eigenvectors for such reduced Hamiltonian problem. These blocks describe the coupling between the very first and the very last thiophene in the polythiophene chain, which are separated by (*N*-1) thiophenes. Next, we replace all couplings and overlap blocks in eq. (5) for thiophenes separated by (*N*-2) and more units and again solve the corresponding eigenvalue problem. We continue the process of reduction and diagonalization until only the coupling between the nearest neighbors is left. The resulting solutions are compared with the reference solution obtained for the full Hamiltonian. In the reduction process the resulting $\overline{H}$ and $\overline{S}$ matrices become banded and sparse, and in the limit where they become diagonal matrices with $\overline{H}$ consisting eigenvalues of the diabatic state which are fully localized

within individual thiophenes while $\overline{S}$ becomes a unit matrix. The reduction process has been designed to expose loss of accuracy in the transition from solution for the full Hamiltonian to the approximate Hamiltonian in the diabatic orbitals representation and to shed light on the effect of space separation and interaction length-scale on the Hamiltonian spectrum.

First, we note that because of planar symmetry of polythiophene (it is coplanar with *y,z*-plane, as shown in Fig. 1b), only p_x orbitals contribute to π-conjugated valence and conduction bands. For the STO-3G basis set there are only six p_x type A.O. per thiophene unit that contribute to π bands, whereas for 6-31G(d) basis set there are 21 basis functions per thiophene ring (11 p_x A.O., 5 d_{xy}, and 5 d_{xz} orbitals) that contribute to π bands. However, in both STO-3G and 6-31G(d) cases only the four lowest energy diabatic π orbitals are occupied and only three of them contribute to valence band. The lowest energy π orbital is localized within the core shell of sulfur and as such it does not contribute to charge transport. The remaining two diabatic π orbitals are unoccupied and contribute to conduction band. That is, the π-conjugated valence and conduction bands in polythiophene are formed through the coupling between five diabatic π orbitals from each thiophene unit. For the 6-31G (d) basis set the valence and conduction π orbitals include contribution from d_{xy} and d_{xz} A.O. but there are still only five diabatic π orbitals per thiophene. We denote these π diabatic orbitals according to increasing MO energy as π-2, π-1, and π (occupied ones) and π* and π* + 1 (unoccupied ones) as shown in Figure 2.

Next a single-point DFT calculation was conducted with quantum chemistry package Q-chem.[32] In particular, a long-range-corrected functional, LRC-ωPBEh[33] with STO-3G and 6-31G(d) basis sets[14] was employed. The generated Fock matrix (FM) and overlap matrix (SM) were used in the following analysis. All p_x orbitals (two from one sulfur atom, four from four carbon atoms) were used to rebuild a new Fock and overlap matrix, namely FM-p_x and SM-p_x, which contained all the most important information of the π orbitals.

The diabatic state for each unit was obtained by the unit block diagonalization scheme. Three steps were carried out here: (1) partitioning the FM and SM into an array of 64 × 64 blocks $\overline{S}_{k,k'}$ and $\overline{H}_{k,k'}$ where k and k' denotes the basis of each thiophene unit in the chain; (2) construction of the diabatic basis set by solving the eigenvalue problem for each unit as prescribed in eq. (4); the corresponding eigenvectors form a localized diabatic basis set; (3) using the eigenvector matrix to rotate the original FM and SM matrix as prescribed in eqs. (8), (9) to produce new matrixes, named FM-diab and SM-diab corresponding to the diabatic states. Then the corresponding diabatic orbital and energy dominated by the p_x atom orbital component were selected and used to build FM-diabp_x and SM-diabp_x that were used to compute the SE and EC.

Time-Evolution of the Hole State

With the diagonal and most nearby neighboring off-diagonal blocks, a diabatic model Hamiltonian was constructed for the 64 thiophene units chain to simulate how an initially localized hole on a single thiophene unit propagates along the chain during 24 fs.

In the quasiparticle picture, an empty state localized within the valence band is considered a hole; whereas a state localized within the conduction band is considered an electron. The time evolution of the particle described by a valence band state represents a diffusion of a hole which is an important process in consideration of charge carrier transport in semiconductors. In general, the time evolution of the initial hole state $\Psi_h(0)$ can be accomplished either through the density matrix propagation or directly through the evolution of the vector state.[34–36] Here we orthogonalize the diabatic basis set obtained with the STO-3G basis set using the Lowdin scheme, $B' = \overline{S}^{-1/2}B$, and then directly evolve vector state $\Psi_h(0)$ in the orthogonal basis set using a time evolution operator

$$\Psi_h(t) = \left(\sum_{k=1}^{5N} \overline{C'}_k \cdot e^{-i\varepsilon_k t/\hbar} \cdot \overline{C}_k'^{\dagger}\right) \Psi_h(0) \qquad (10)$$

where k runs over all eigenvectors obtained from solution of eq. (6) and $\overline{C}'_k$ denotes k-th eigenvector in a Lowdin orthogonalized basis set B' and ε_k is a corresponding eigenvalue. The dagger symbol in the superscript denotes Hermitian conjugation.

The initial hole state $\Psi_h(0)$ for time propagation was prepared using HOMO-orbital (π diabatic orbital) of the unit-32 thiophene-ring. Note that this diabatic HOMO is not an eigenstate of the full 64-unit Hamiltonian. Moreover, it has non-zero coupling to all diabatic HOMOs (π-2, π-1, and π) and LUMOs (π* and π* + 1) from neighboring thiophene units as will be shown below. The strongest coupling is between HOMO–HOMO and HOMO–LUMO (π-π and π-π*) of neighboring units as will be shown below. That is, the HOMO diabatic orbital, while being fully localized within a single thiophene unit, is not an eigenstate of the full 64-unit large Hamiltonian but rather a superposition of the M.O. from the valence band and with a small mixture of a conduction band state. To prepare a proper initial hole state for the dynamics we removed unwanted conduction band contribution from the HOMO diabatic state $B\prime_{32}^{\mathrm{HOMO}}$ localized in thiophene unit 32 by projecting it onto valence band of the full Hamiltonian from eq. (6) and renormalizing it:

$$\Psi_h(0) = \overline{N}^{-1}\,\overline{C'}_{\mathrm{occ}}\overline{C'}^{\dagger}_{\mathrm{occ}}\,B\prime_{32}^{\mathrm{HOMO}} \qquad (11)$$

where $B\prime_{32}^{\mathrm{HOMO}}$ is a diabatic HOMO orbital of the thiophene unit 32 and $\overline{C'}_{\mathrm{occ}}$ is an array sized (5 * N) × (3 * N) of M.O. coefficients corresponding to (3*N) occupied orbitals from solution of eq. (6). $\overline{C'}^{\dagger}_{\mathrm{occ}}$ is a hermitian conjugation of $\overline{C'}_{\mathrm{occ}}$ and $\overline{C'}_{\mathrm{occ}}\overline{C\prime}^{\dagger}_{\mathrm{occ}}$ is a projector on the valence (occupied) band and the parameter $\overline{N}$ is normalization factor equal to

$$\overline{N} = \sqrt{\left(\overline{C'}_{\mathrm{occ}}\overline{C\prime}^{\dagger}_{\mathrm{occ}}\,B\prime_{32}^{\mathrm{HOMO}}\right)^{\dagger}\left(\overline{C'}_{\mathrm{occ}}\overline{C'}^{\dagger}_{\mathrm{occ}}\,B\prime_{32}^{\mathrm{HOMO}}\right)} \qquad (12)$$

The time evolution given by eq. (10) can be evaluated iteratively with a time step Δt. The resulting survival probabilities

for the thiophene unit 32 and the sequence of probability transfers to neighboring thiophenes and corresponding CT rates contain information about hole diffusion. A similar methodology can be applied to model electron diffusion in the conducting band.

Results and Discussion

Note that the current research work only focused on presenting a calculation method and demonstrating that it is a fast means to obtain the ECs for CT; the method and research is not aiming at quantitatively comparing with experimental measurements. To that end, a small STO-3G basis set and a medium 6-31G (d) basis set were used, which are simple but adequate enough to illustrate how the method works.

Each thiophene unit contained 42 electrons and 31 A.O. in the calculation, and the overall size of the FM and SM was 1986 × 1986 for the STO-3G basis set and 5316 × 5316 for the 6-31G(d) basis set. Because of the planar symmetry of polythiophene, we adopt a σ-π separation approach, where only p_x symmetry orbitals that can contribute to valence and conduction bands (π orbitals) are taken into account. For the STO-3G basis set each carbon contributes one p_x orbital, whereas sulfur can contribute two p_x orbitals ($2p_x$ and $3p_x$), totaling six p_x orbitals per thiophene ring. The $2p_x$ orbital of sulfur was included in the current benchmarks to verify its contribution to delocalized valence and conduction orbitals. The corresponding size of submatrixes with the selected FM-p_x and SM-p_x was 384 × 384 with 6 p_x orbitals per unit scheme. For the 6-31G(d) basis set the diabatic π orbitals include small contributions from d_{xy} and d_{xz} A.O. Overall, there are a total of 21 A.O. of p_x, d_{xy}, and d_{xz} per thiophene unit but only 5 π orbitals contribute to valence and conduction bands. Since no s, p_y, p_z, or the remaining d-type orbitals contributed to the delocalized π orbital in the chain, after diagonalizing the FM-p_x and SM-p_x matrices, we obtained the eigen-energies of the conjugated π orbitals, which were exactly the same as the corresponding orbital energies obtained from Q-Chem calculations, showing that the σ-π separation approach is valid. These π orbital eigen-energies were used as benchmarks for the following diabatization analysis. In both the STO-3G and 6-31G(d) cases, there are only 320 orbitals (5 per thiophene unit) that are needed for the description of hole dynamics.

After the diabatization, the local diabatic states for each unit were generated. For example, for the STO-3G basis set, the six diabatic orbitals containing sulfur and carbon p_x orbitals are labeled as π-3, π-2, π-1, π, π*, and π*+1 by increasing energy order. These orbitals correspond, respectively, to HOMO-13, HOMO-5, HOMO-1, HOMO, LUMO, and LUMO+1. Note that the HOMO-13 is formed by the low-lying $2p_x$ lone pair orbital of a sulfur atom. The ordering can change depending on basis set used. To illustrate these STO-3G diabatic π orbitals that contribute to valence and conduction bands, their shapes are displayed in Figure 2 using a single thiophene ring calculation. It can be seen that all of these orbitals are π-type orbitals, as indicated by the node in the molecular plane. In addition, the number of nodes perpendicular to the molecular plane increases from 0 for HOMO-5, to 1 for HOMO-1 and HOMO, and to 2 for LUMO and LUMO+1 with increasing orbital energies. It is worth emphasizing that HOMO-1 is different from the rest in that the nodal plane passes through the two carbon atoms at the alpha-position to sulfur. This may lead to negligible ECs between neighboring thiophene units. In addition, the orbital lobes on the two carbon atoms at alpha-position to sulfur are apparently greater for HOMO than LUMO and LUMO+1. Such a difference may lead to larger ECs for HOMO than the unoccupied orbitals. The diabatic π orbitals for 6-31G(d) basis set look similar to the ones shown in Figure 2.

The diabatic Hamiltonian matrix FM-diab contains the information needed in order to calculate and understand the kinetics and dynamics of the CT along the chain. Specifically, the diagonal block provides orbital SE for each unit, and the off-diagonal block corresponds to the ECs between any unit pair in the chain. Due to the symmetry of the molecular chain, the diabatic orbital SE for each unit is the same except for those which were close to the two ends of the chain, whose energies were relatively higher due to the terminal effect. The results of the site energies for STO-3G and 6-31G(d) basis sets are depicted in Figure 3, where five of the π orbitals' site energies for the 64 units were presented. Increasing the size of the basis set from STO-3G to 6-31G(d) lowers the orbital energies. This is expected on the base of variational principle. The different site

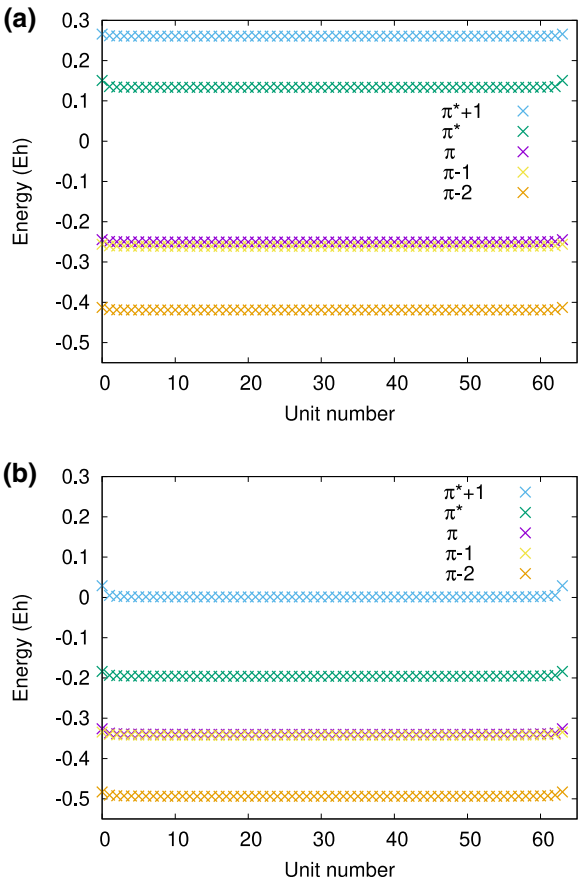

Figure 3. The diabatic orbital site energy for each unit along the chain for a) STO-3G basis set and b) 6-31G(d) basis set. Note, that the site energies near units 1 and 64 increase suggesting possible hole trapping at the polymer chain edges. [Color figure can be viewed at wileyonlinelibrary.com]

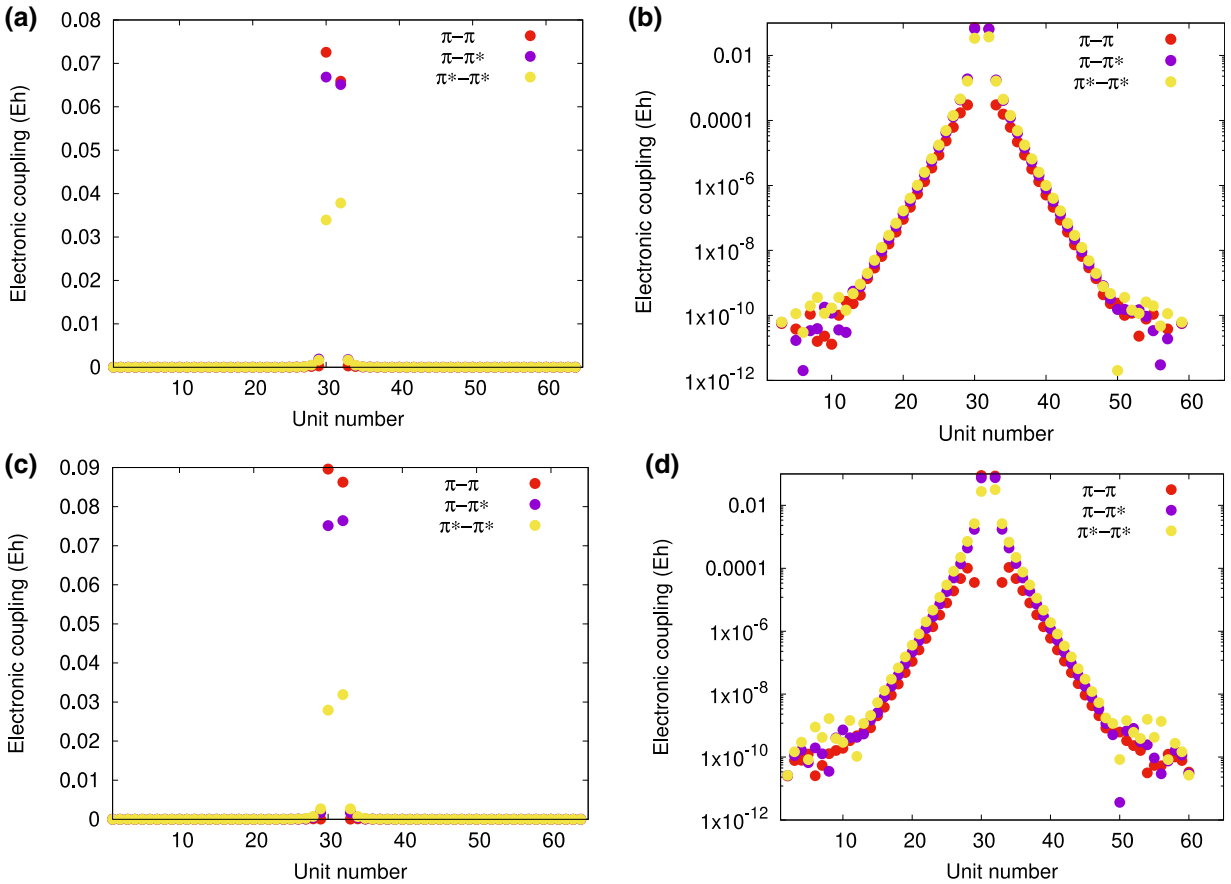

Figure 4. The electronic couplings between unit 31 and the other units in the chain for STO-3G basis set a) and b) and for 6-31G(d) basis set c) and d). The coupling elements show exponential decay which is demonstrated by its linear dependence on the logarithmic scale b) and d). Only diabatic π-π, π-π*, and π*-π*, were selected as examples. The coupling from other orbital pairs had a similar trend. [Color figure can be viewed at wileyonlinelibrary.com]

energies for the hydrogen-terminated end-units suggest that the charge carriers (holes and/or electrons) can be trapped at the edges. Such charge trapping at the edges has indeed been observed experimentally.[37,38] Nevertheless, the constant SE in the middle section of the chain offers a convenient parameter for the study of kinetics and dynamics.

To examine the EC for different coupling pairs, extracted from off-diagonal blocks in FM-diab, in particular, we selected the 31st thiophene unit, and calculated its pairwise EC with all the other units, as shown in Figure 4. Note that the EC depends on the separation distance between the two coupled units. As shown in Figure 4, the coupling energies for π-π, π-π*, and π*-π* all sharply decrease with increasing separation between the two units. The linear behavior on the logarithmic scale (panels b and d) shows that the decay is in fact exponential. The largest coupling exists between the most nearby two neighboring units, such as unit 31 and 30, and unit 31 and 32. Note that in the thiophene chain, the angles of S-C-left unit and S-C-right unit were not the same. This inhomogeneous structure profile explains why the coupling values between 31–30 and 31–32 pairs were not exactly identical in Figure 4. The π-π coupling for the thiophene units with larger separation was <0.0003 Eh, and quickly decayed to zero. For π*-π* and π-π*, the coupling was smaller, and beyond unit 32 and beyond unit 30, the coupling with unit 31 was < 0.0019 Eh. Also displayed as a logarithm scale in Figures 4b and 4d, the π*-π* coupling persisted for larger separation units. The results suggest that the couplings from the nearest neighboring units dominate and need to be considered in the CT calculations, and the EC from other further-away units can be ignored.

Additional evidence for the nearest neighboring contribution can be obtained by fitting the frontier orbital energies for the polymer chains. Figure 5 shows the evolution of five π orbitals into π bands as the number of units *N* increases from 1 through 64. The Density of States (DOS) for these π bands calculated with 6-31G* basis agrees well with experimental ultraviolet photoemission spectroscopy and inverse photoemission spectroscopy data for P3HT, in terms of not only the prominent features including van Hove singularities and high DOS peaks but also the separations between the valence band maximum or conduction band maximum and the high DOS peaks of the occupied and unoccupied states.[39] The π-2 orbital for $N = 1$ is low in energy and remains isolated and even developed into a wide band for $N = 64$. In comparison, π and π-1 are close in energy for $N = 1$, and therefore, as these two orbitals developed into π bands for $N = 64$ they unavoidably overlap each other. However, as discussed above, the nodal plane of π-1 passes through the two carbon atoms at the alpha-position to sulfur and therefore the π-1 derived band width should be small. Consequently, the top of the valence bands for $N = 1$ to

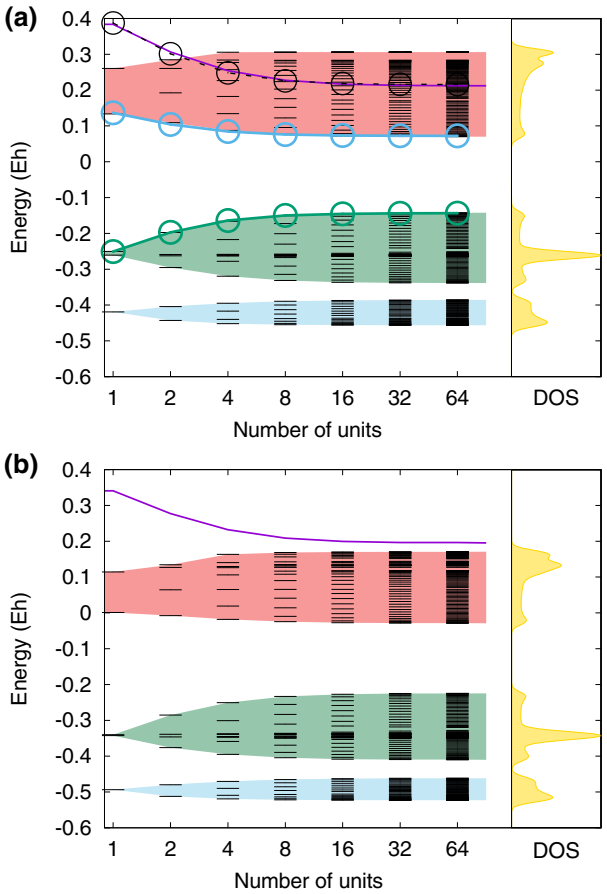

Figure 5. M.O. energies as a function of the number of thiophene units calculated with a) STO-3G basis set and b) 6-31G(d) basis set. Three non-overlapping bands are formed from p_x orbitals in polythiophene. Black horizontal dashes: M.O. energies. Light-red shaded region: conduction band, light-green and light-blue shaded regions: valence bands. Purple solid curve corresponds to the HOMO–LUMO gap (bandgap) as a function of thiophene unit number. The fit of HOMO (top of the valence band), LUMO (bottom of the conduction band), and HOMO–LUMO gap (bandgap, as indicated by black dashed curve) for the STO-3G basis set to the simple form of eqs. (13), (14) is shown as curves and emphasized with circles. The corresponding DOS are shown on the right. [Color figure can be viewed at wileyonlinelibrary.com]

64 should be only associated with π (indicated by circles in Fig. 5). Although the energy separation between π* and π*+1 is relatively large, the bands derived from these two orbitals appear to overlap each other. However, the bottom of the conduction bands should be only associated with the π*.

These orbital characteristics allow us to fit the frontier orbital energies using a tight-binding model:

$$E_v = \alpha_v + 2|\beta_v|\cos[\pi/(N+1)] \quad (13)$$

$$E_c = \alpha_c - 2|\beta_c|\cos[\pi/(N+1)] \quad (14)$$

where α and β represent site energies and ECs, respectively, and subscripts v and c stand for valence and conduction bands. For convenience, we avoid running into the sign issue by using the absolute value of the ECs. Fitting for the STO-3G results gave α_v = −0.2508, β_v = 0.0537, α_c = 0.1367, and β_c = 0.0323 Eh, with good fitting qualities as measured by R^2 = 0.999 and 0.985, respectively. It is notable that the band gap E_g is very well reproduced by using these tight-binding parameters. The site energies α_v and α_c from fit also agree very well with those values directly obtained from diabatization process equal to −0.2581 Eh and 0.1338 Eh for, respectively, p and p* diabatic orbital (Fig. 3). However, the agreement with the ECs shown in Figure 4 is not as good. The difference is most likely due to the fact that the tight-binding model does not include coupling between orbitals with different energies, which are not completely negligible as can be seen from the π-π* (HOMO–LUMO) coupling in Figure 4. Nevertheless, these results indicate that the first neighbors are the most important sites to contribute to the ECs.

To further validate that only the nearest neighboring unit coupling should be considered in the CT calculation, we reconstructed a series of model Hamiltonians of the molecule by deleting the off-diagonal coupling blocks in FM-diabp$_x$ beginning from the one farthest away to the diagonal blocks until reaching the blocks that were the nearest neighbors to the diagonal blocks. The eigen-energies of these model Hamiltonians were plotted in Figure 6. It shows that by just including a few neighboring couplings, it can reproduce the eigen-energies generated by the full DFT calculations (Figs. 6a and 6b). Furthermore, the mean unsigned error of the eigen-energies for only including the most nearby neighboring couplings was <0.00006 Eh, while the error for HOMO-orbital and LUMO-orbital energies was highlighted in Figure 6c. The results support the conclusion that the EC between the nearest neighboring units is adequate for the CT kinetic and dynamics calculations.

Finally, we note that sulfur atom's 2p$_x$ orbital had too low energy (c.a. −5.78 Eh and −6.03Eh for, STO-3G and 6-31G(d) basis sets, respectively) and formed a lone pair orbital with itself, instead of forming a conjugated π orbital. Therefore, we repeated the previous validation discussed above for the diabatization analysis using 3p$_x$ from the sulfur atom, and all the 2p$_x$ from the carbon atoms, which we call the five-orbitals scheme. By comparing the FM-diabp$_x$ with six orbitals (6o) and five-orbitals (5o) schemes, we obtained very similar results. For instance, Figure 7 displays the eigen-energy by diagonalizing FM-diabp$_x$ constructed with both 6o and 5o for the STO-3G basis set. It was found that their energies were exactly the same, except for the ones around −5.78 Eh, which were solely contributed by sulfur atom's 2p$_x$ orbital. Meanwhile, the reduction of the number of orbitals can significantly improve the calculation efficiency in the following CT dynamics simulations, especially for a large system.

Figure 8 displays results of quantum dynamics simulations for a propagating hole which was initially constructed from the HOMO-orbital of the thiophene-ring for unit-32. During the 24-fs time evolution, it was observed that the hole became delocalized very quickly. Note that time evolution of survival probability of a hole occupying the initial HOMO orbital (Fig. 8a) and occupying the unit-32 was studied (Fig. 8b). The survival probability occupying unit-32 was defined as the sum of the probability of the five orbitals within unit-32. Within 2 fs, a significant decay of both of the survival probability was found. However, the decay did not reach to a constant-zero, and in contrast an oscillation pattern was observed during the propagation, which demonstrated that the hole had a probability of coming back to the initial orbital or unit. This

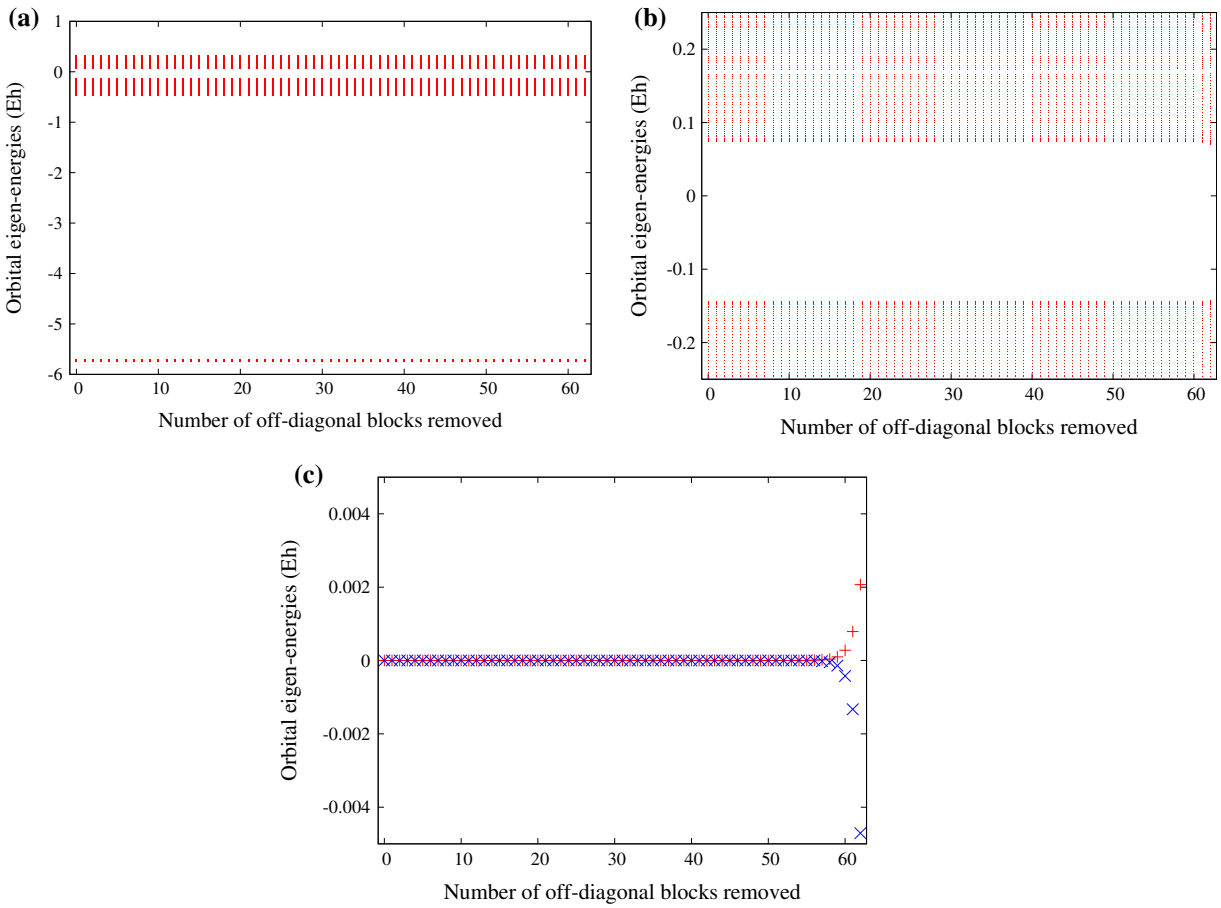

Figure 6. The eigen-energies of the 63 model Hamiltonians for the STO-3G basis set. The ones displayed at zero were the references obtained by full FM-diabp$_x$ a) and b). The right one b) is a zoom in of the range close to the HOMO–LUMO gap. The bottom one c) shows the error for the diabatic π and π* orbitals (red and blue, respectively). [Color figure can be viewed at wileyonlinelibrary.com]

phenomenon is due to the coherent hole transfer mechanism, since we fixed the nuclear degree of freedom, thus no dissipation or relaxation was included in the present simulation. Furthermore, different propagations with different coupling strengths (half of and double the original couplings) were investigated. As expected, with larger couplings, faster delocalization and faster oscillation can be found in the simulation, as shown in Figure 8 in blue. Conversely, for the one with smaller coupling, the dynamics significantly slowed down and had suppressed oscillation, as shown in Figure 8 in green. Meanwhile, we noticed that there was no significant difference of delocalization with respect to the orbital or the entire unit. This was because within the five orbitals in the same unit, they would not directly interact with each other.

The current approach for time evolution of the hole in the valence band or electron in the conduction band can be extended to include time-dependence of coupling elements and of the diabatic on-site energies due to vibrational/thermal motion of thiophene rings and phonon modes of the polythiophene or external perturbation. Such extension, while requiring the Hamiltonian to be recalculated and hence increasing the computational time, provides a promising way for a real-time modeling of phonon assisted charge transport, charge carrier injection or non-radiative recombination of electron and hole.

To estimate the effect of conformational flexibility in polythiophene and its thermal motion on the charge transport dynamics we performed a 10 ps classical molecular dynamics (MD) simulations of 64-unit thiophene chain at constant temperature of 298.15 K. In the MD simulations, five 64-unit polythiophene chains were used, and they were arranged by putting one chain in the center and the other four aligned on

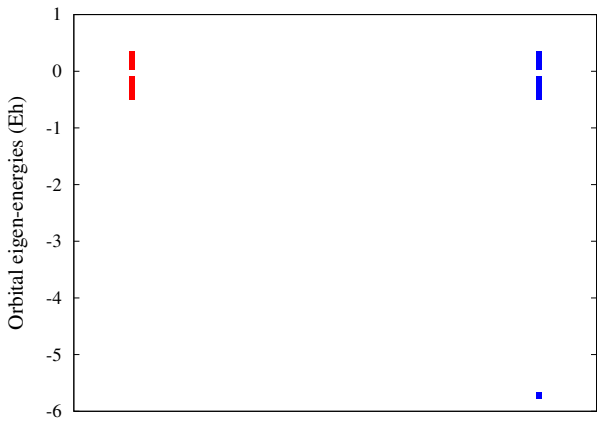

Figure 7. The eigen-energies obtained by the 5o scheme (blue) and 6o scheme (red) illustrated using the STO-3G basis set. [Color figure can be viewed at wileyonlinelibrary.com]

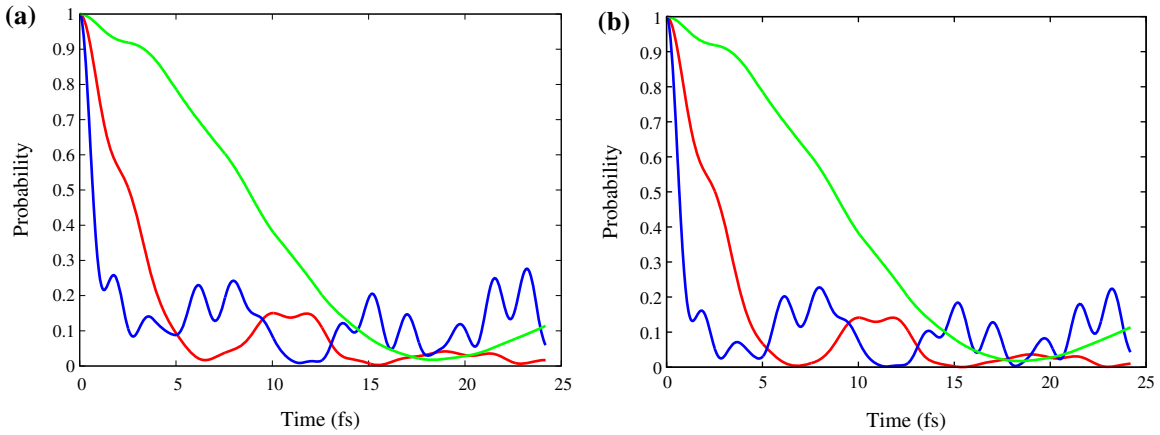

Figure 8. The time evolution of survival probability of a hole occupying the unit-32 a) and occupying the π orbital (HOMO) of unit 32 b) calculated using the electronic couplings from the STO-3G basis set. The survival probability occupying unit 32 was defined as the sum of the probability of the five orbitals in the unit-32. The green, red, and blue curves corresponded to the simulations with 0.5×, 1×, and 2× of the original electronic couplings. [Color figure can be viewed at wileyonlinelibrary.com]

the top, bottom, front, and back to mimic the crystal environment. By fixing the surrounding four chains and relaxing the one in the center, we collected 10 frames (one frame per ps) along the trajectory. By doing statistical analysis for the couplings calculated with the STO-3G basis for the 10 frames, each of which contains 61 most nearby unit pairs without containing the two ending units, the average and standard deviation of the π-π, π-π*, and π*-π* couplings were 0.039599 ± 0.018994 Eh, 0.050570 ± 0.015201 Eh, and 0.036925 ± 0.002205 Eh. Such fluctuations represent the effect of the nuclear degrees of freedom that can be used to model loss of coherence and transition between different bands.[40] More accurate models may include explicit motion of the nuclei and non-adiabatic couplings which are required to model dissipation of energy from the excited electronic structure to the nuclei. Finally, a screened Coulomb potential is required to model processes that involve multiple charge carriers such as exciton formation of dissociation and are beyond the scope of this work.

Conclusion

We have presented a simple, efficient, and robust means to construct the diabatic states and their ECs for very large molecules by combining DFT electronic structure calculations and block diagonalization. This method was tested for a thiophene-ring system that models a P3HT polymer chain, and the energy information calculated was used to simulate a hole transfer process for tens of femtoseconds. We conclude that: (1) using the minimal number of diabatic orbitals in the calculations can correctly reproduce the electronic energy benchmarked by DFT calculations; (2) using diabatic orbitals has advantages over using A.O. in the coupling calculations, since the former choice can be easily extended to more complicated large molecules, where it is difficult to filter out the A.O. which contribute to the CT; (3) the method can obtain all the EC information between any thiophene pairwise units which were not necessarily close to each other, and it was demonstrated that with more coupling terms included, the more accurate the electronic energy generated; (4) a good approximation is obtained by only considering the couplings between the most nearby neighboring units for CT calculations; and (5) site energies for the terminal thiophenes in the polythiophene chain differ from the rest of the chain which suggest a role in charge trapping at the crystal edges.

Overall, the proposed diabatic basis decomposition is a promising path forward for real-time modeling of a phonon assisted charge transport, charge carrier injection, or non-radiative recombination of electrons and holes. We note that our diabatization scheme is exact, regardless of the model chemistry used. The only approximations are the σ-π separation, neglect of the ECs between distant neighbors, and truncations from 6 to 5 π orbitals, which show minor effects on the site energies and coupling constants if calculations are property done. Since the DFT functional we used for the calculations has already been validated during its development stage using experimental data for ionization potential, electron affinity, and CT,[33] the site energies and coupling constants extracted from our diabatization scheme can be used with confidence to predict experimental phenomenon.

Acknowledgments

This work was conducted at the Center for Nanophase Materials Sciences, a US Department of Energy Office of Science User Facility and was sponsored by the Laboratory Directed Research and Development (LDRD) Program of Oak Ridge National Laboratory. This work used the Extreme Science and Engineering Discovery Environment (XSEDE), which is supported by National Science Foundation Grant No. ACI-1548562 (allocation TG-DMR110037). Tao Yu acknowledges the Department of Energy Visiting Faculty Program (VFP) at ORNL. Jacek Jakowski is grateful for the time spent at Emory University from 2007 to 2010 during which he collaborated with Prof. Keiji Morokuma on development of real-time Liouville-von Neumann electron dynamics and density functional tight binding approaches.

Keywords: band structure · electronic structure · quantum dynamics · DFT · conducting polymers

How to cite this article: T. Yu, F. Fabunmi, J. Huang, B. G. Sumpter, J. Jakowski. *J. Comput. Chem.* **2019**, 40, 532–542. DOI: 10.1002/jcc.25749

[1] C. W. Tang, *Appl. Phys. Lett.* **1986**, *48*, 183.
[2] A. Facchetti, *Chem. Mater.* **2011**, *23*, 733.
[3] J. E. Anthony, *Chem. Rev.* **2006**, *106*, 5028.
[4] A. Marrocchi, D. Lanari, A. Facchetti, L. Vaccaro, *Energy Environ. Sci.* **2012**, *5*, 8457.
[5] S. Ludwigs, *Adv. Polym. Sci.* **2014**, *265*, 107.
[6] T. Yamamoto, K. Sanechika, A. Yamamoto, *J. Polym. Sci., Part C: Polym. Lett.* **1980**, *18*, 9.
[7] J. A. Lim, F. Liu, S. Ferdous, M. Muthukumar, A. L. Briseno, *Mater. Today* **2010**, *13*, 14.
[8] V. Coropceanu, J. Cornil, D. A. da Silva, Y. Olivier, R. Silbey, J. L. Bredas, *Chem. Rev.* **2007**, *107*, 926.
[9] V. Coropceanu, H. Li, P. Winget, L. Y. Zhu, J. L. Bredas, *Annu. Rev. Mater. Res.* **2013**, *43*, 63.
[10] B. Kippelen, J. L. Bredas, *Energy Environ. Sci.* **2009**, *2*, 251.
[11] L. Wang, J. Jakowski, S. Garashchuk, B. G. Sumpter, *J. Chem. Theory Comput.* **2016**, *12*, 4487.
[12] Z. Hu, J. Jakowski, C. Zheng, C. J. Collison, J. Strzalka, B. G. Sumpter, R. Verduzco, *J. Polym. Sci., Part B: Polym. Phys. Ther.* **2018**, *56*, 1135.
[13] J. Jakowski, J. S. Huang, S. Garashchuk, Y. D. Luo, K. L. Hong, J. Keum, B. G. Sumpter, *J. Phys. Chem. Lett.* **2017**, *8*, 4333.
[14] W. J. Hehre, R. F. Stewart, J. A. Pople, *J. Chem. Phys.* **1969**, *51*, 2657.
[15] E. F. Valeev, V. Coropceanu, D. A. da Silva, S. Salman, J. L. Bredas, *J. Am. Chem. Soc.* **2006**, *128*, 9882.
[16] M. J. Frisch, J. A. Pople, J. S. Binkley, *J. Chem. Phys.* **1984**, *80*, 3265.
[17] W. J. Hehre, R. Ditchfield, J. A. Pople, *J. Chem. Phys.* **1972**, *56*, 2257.
[18] W. J. Hehre, W. A. Lathan, *J. Chem. Phys.* **1972**, *56*, 5255.
[19] W. J. Hehre, J. A. Pople, *J. Chem. Phys.* **1972**, *56*, 4233.
[20] P. O. Lowdin, *J. Chem. Phys.* **1950**, *18*, 365.
[21] V. Prucker, O. Rubio-Pons, M. Bockstedte, H. B. Wang, P. B. Coto, M. Thoss, *J. Phys. Chem. C* **2013**, *117*, 25334.
[22] J. R. Li, H. B. Wang, P. Persson, M. Thoss, *J. Chem. Phys.* **2012**, *137*, 22A529.
[23] G. H. Wannier, *Phys. Rev.* **1937**, *52*, 0191.
[24] W. Kohn, *Phys. Rev.* **1959**, *115*, 809.
[25] J. D. Cloizeaux, *Phys. Rev.* **1963**, *129*, 554.
[26] M. Elstner, G. Seifert, *Philos. Trans. R. Soc. A* **2014**, *372*, 21020483.
[27] Q. Cui, M. Elstner, *Phys. Chem. Chem. Phys.* **2014**, *16*, 14368.
[28] M. Gaus, Q. Cui, M. Elstner, *Wires Comput. Mol. Sci.* **2014**, *4*, 49.
[29] G. S. Zheng, M. Lundberg, J. Jakowski, T. Vreven, M. J. Frisch, K. Morokuma, *Int. J. Quantum Chem.* **2009**, *109*, 1841.
[30] V. Coropceanu, T. Nakano, N. E. Gruhn, O. Kwon, T. Yade, K. Katsukawa, J. L. Bredas, *J. Phys. Chem. B* **2006**, *110*, 9482.
[31] D. Dudenko, A. Kiersnowski, J. Shu, W. Pisula, D. Sebastiani, H. W. Spiess, M. R. Hansen, *Angew. Chem., Int. Ed.* **2012**, *51*, 11068.
[32] Y. Shao, L. F. Molnar, Y. Jung, J. Kussmann, C. Ochsenfeld, S. T. Brown, A. T. B. Gilbert, L. V. Slipchenko, S. V. Levchenko, D. P. O'Neill, R. A. DiStasio, R. C. Lochan, T. Wang, G. J. O. Beran, N. A. Besley, J. M. Herbert, C. Y. Lin, T. Van Voorhis, S. H. Chien, A. Sodt, R. P. Steele, V. A. Rassolov, P. E. Maslen, P. P. Korambath, R. D. Adamson, B. Austin, J. Baker, E. F. C. Byrd, H. Dachsel, R. J. Doerksen, A. Dreuw, B. D. Dunietz, A. D. Dutoi, T. R. Furlani, S. R. Gwaltney, A. Heyden, S. Hirata, C. P. Hsu, G. Kedziora, R. Z. Khalliulin, P. Klunzinger, A. M. Lee, M. S. Lee, W. Liang, I. Lotan, N. Nair, B. Peters, E. I. Proynov, P. A. Pieniazek, Y. M. Rhee, J. Ritchie, E. Rosta, C. D. Sherrill, A. C. Simmonett, J. E. Subotnik, H. L. Woodcock, W. Zhang, A. T. Bell, A. K. Chakraborty, D. M. Chipman, F. J. Keil, A. Warshel, W. J. Hehre, H. F. Schaefer, J. Kong, A. I. Krylov, P. M. W. Gill, M. Head-Gordon, *Phys. Chem. Chem. Phys.* **2006**, *8*, 3172.
[33] M. A. Rohrdanz, K. M. Martins, J. M. Herbert, *J. Chem. Phys.* **2009**, *130*, 054112.
[34] J. Jakowski, S. Irle, B. G. Sumpter, K. Morokuma, *J. Phys. Chem. Lett.* **2012**, *3*, 1536.
[35] J. Jakowski, S. Irle, K. Morokuma, *Phys. Chem. Chem. Phys.* **2012**, *14*, 6273.
[36] J. Jakowski, K. Morokuma, *J. Chem. Phys.* **2009**, *130*, 224106.
[37] M. Setvin, X. F. Hao, B. Daniel, J. Pavelec, Z. Novotny, G. S. Parkinson, M. Schmid, G. Kresse, C. Franchini, U. Diebold, *Angew. Chem., Int. Ed.* **2014**, *53*, 4714.
[38] T. He, Y. F. Wu, G. D'Avino, E. Schmidt, M. Stolte, J. Cornil, D. Beljonne, P. P. Ruden, F. Wurthner, C. D. Frisbie, *Nat. Commun.* **2018**, *9*, 2141.
[39] K. Kanai, T. Miyazaki, H. Suzuki, M. Inaba, Y. Ouchib, K. Seki, *Phys. Chem. Chem. Phys.* **2010**, *12*, 273.
[40] X.-K. Chen, J.-L. Bredas, *Adv. Energy Mater.* **2018**, *8*, 1702227.

Received: 30 June 2018
Revised: 8 October 2018
Accepted: 10 October 2018
Published online in Wiley Online Library